Biosensors and Bioelectronics 129 (2019) 175–181

Contents lists available at ScienceDirect

Biosensors and Bioelectronics

journal homepage: www.elsevier.com/locate/bios

A flyover style microfluidic chip for highly purified magnetic cell separation

Shujing Lin[a,b,c,1], Xiao Zhi[d,1], Di Chen[a,b,c,*], Fangfang Xia[a], Yihuan Shen[a], Jiaqi Niu[a], Shiyi Huang[d], Jie Song[a,b,c], Jianmin Miao[e], Daxiang Cui[a,b,c], Xianting Ding[d]

[a] School of Electronic Information and Electrical Engineering, Shanghai Jiao Tong University, Shanghai 200240, PR China
[b] Shanghai Engineering Research Center for Intelligent Diagnosis and Treatment Instrument, Shanghai 200240, PR China
[c] Key Lab. for Thin Film and Microfabrication Technology of Ministry of Education, Shanghai 200240, PR China
[d] School of Biomedical Engineering, Institute for Personalized Medicine, Shanghai Jiao Tong University, Shanghai 200030, PR China
[e] School of Mechanical and Aerospace Engineering, Nanyang Technological University, Singapore 639798, Singapore

ARTICLE INFO

Keywords:
Microfluidic chip
Magnetic separation
Continuous flow
Cell sorting

ABSTRACT

White blood cells (WBCs) isolated from peripheral blood have been verified as important biomarkers for the diagnosis, treatment and prognosis of cancer. However, it's still under challenge to acquire high-purity WBCs, even by taking advantage of current microfluidic technology. Considering the universality of clinical magnetic activated cell sorting (MACS) method, new developments on microfluidic chip in combination of magnetic cells separation technologies may provide a fascinating approach for high-purity WBCs sorting and widely clinical application. Here, we present a flyover style microfluidic chip which has been elaborately embedded with two-stage magnetic separation in continuous flow for WBCs sorting. Immunomagnetic micro/nano-particles (IMNPs) labeled WBC (WBC@IMNPs) were sequentially separated by a lateral magnetic force and a vertical magnetic force, and the final separation purity of WBCs reached up to 93 ± 1.67% at a flow rate of 20 μL min^{-1}. Furthermore, the WBCs viability was up to 97.5 ± 1.8%. Consequently, this novel flyover style microfluidic-chip with magnetic separation technology has been successfully demonstrated as cut-in-edge method for high-purity WBCs sorting, and obviously it's easy to extend for other types of cells sorting under great potential application in biomedical fields.

1. Introduction

Blood cell separation is an essential and critical step in clinical diagnosis and therapeutic regimens, because each blood component is capable of carrying certain important heath information (Gossett et al., 2010; Plouffe and Murthy, 2014). White blood cells (WBCs) are vital components of blood and act as defenders to fight against infections (such as acquired immune deficiency syndrome (AIDS), tuberculosis, or herpes simplex, malaria). Abnormal levels or deformations of WBCs are closely related to immune disorder, infection or cancer (Nivedita and Papautsky, 2013; Wu et al., 2012), therefore, WBCs can be as significant indications for clinical diagnosis or treatment (Brunstein et al., 2015; Kim et al., 2016). For instance, $CD8^+$ T cells, one of the subtypes of WBCs, are an effective response to hepatitis B virus (HBV) (Maini et al., 2000). CD4/CD8 ratio may prove useful in monitoring response to antiretroviral therapy of human immunodeficiency virus (HIV) (Doitsh et al., 2013; Serrano-Villar et al., 2014). WBCs also play a key role in the therapy of cancer and type 1 diabetes (Delong et al., 2016; Joyce and Fearon, 2015). High-purity WBCs separation from whole blood can facilitate accurate diagnosis in precision medicine (Ahmed et al., 2017; Poudineh et al., 2017; Zhang et al., 2017). In general, there are two conventional methods for blood cell separation: flow cytometry and centrifugation. However, these technologies require costly instrumentation, skilled operators, massive sample and multiple processes. More importantly, these means still have shortcomings of low purity, low efficiency and cell damages (Gholizadeh et al., 2017; Wu et al., 2016).

In last decades, for the purpose of cells separation of high purity, high efficiency, high-throughput, and low-cost, a variety of approaches had been developed, such as centrifugal separation (Russom et al., 2009), inertial separation (Abdulla et al., 2018; Wu et al., 2016), physical filtration (Adams et al., 2014; Chen et al., 2014), dielectrophoresis (DEP) separation (Chen et al., 2018), optical isolation (Wang et al., 2011), optoelectronic tweezers (Jeorrett et al., 2014), acoustic cell sorting (Ding et al., 2012) and magnetic activated cell sorting (MACS) (Hyun et al., 2015). In particular, MACS is the most

* Corresponding author at: School of Electronic Information and Electrical Engineering, Shanghai Jiao Tong University, Shanghai 200240, PR China.
E-mail address: dchen@sjtu.edu.cn (D. Chen).
[1] Equal contributors.

https://doi.org/10.1016/j.bios.2018.12.058

Available online 30 January 2019

potential technique for separating target cells from a farraginous cell population, due to its outstanding advantages of contactless, highly specificity and high-throughput sorting (Bhuvanendran Nair Gourikutty et al., 2016; Iranmanesh and Hulliger, 2017). MACS typically utilizes antibodies-labeled magnetic particles to specifically capture, and then separate captured cells by an external magnetic field (Zeng et al., 2013). Thus, magnetic field distribution is a critical factor that need to be considered and designed carefully. In previously works, permanent magnets (Lipfert et al., 2009) or electromagnets (Haber and Wirtz, 2000) were applied to generating desirably magnetic field for cell sorting. Although soft (Liu et al., 2009) or permanent (Osman et al., 2013) magnetic microstructures were also designed to enhance the local magnetic field gradient for higher separation efficiency, there still is a space for further improvement in the separation efficiency (Hejazian et al., 2015). Nowadays, several commercial products (such as Cellsearch®, CliniMACS®, DynaMag™) also had been applied for separating WBCs from peripheral blood. But, the low separation purity, low recovery rate and high cost limit their applications. Microfluidic chip, which can offer precise microfluidic control and less reagent cost, had been proven suitable for cells separation (Yu et al., 2014). Thereby, microfluidic chips were introduced into MACS flied in variety of ways (Warkiani et al., 2015). Yet, some challenges, such as low separation efficiency and purity, still need to be further overcome in MACS area (Plouffe et al., 2014; Welzel et al., 2015).

Herein, we presented a continuous-flow two-stage separation strategy of lateral separation and vertical separation in a flyover style microfluidic chip to realize high-purity WBCs separation. At the first stage, lateral magnetic zone that integrates a soft magnetic structure was designed to enrich target cells and improve the recovery rate. At the second stage, vertical magnetic zone, which is a flyover-like three-dimensional (3D) microchannel structure, was designed for further enhancing the purity of WBCs. As a proof-of-concept demonstration for our flyover structural microfluidic chip, high-purity WBCs were successfully separated from peripheral blood at different flow rate (20, 30, 40, 50, 60 μL min^{-1}).

2. Theoretical and design principle

2.1. Theoretical

MACS in microfluidic chip involves two important aspects of magnetism and fluid mechanics in microscale (Nguyen, 2011). To reach high separation efficiency and purity, forces acted on the WBC@IMNPs firstly need to be understood. Here, we assume a WBC@IMNPs is a sphere. According to Newton's second law, the equation of forces on a WBC@IMNPs is (Hejazian et al., 2015):

$$m_c \frac{d\boldsymbol{u}_c}{dt} = \boldsymbol{F}_m + \boldsymbol{F}_{dw} + \boldsymbol{F}_d + \boldsymbol{F}_B + \boldsymbol{F}_l \quad (1)$$

Where m_c, $\boldsymbol{u}_c$, $\boldsymbol{F}_m$, $\boldsymbol{F}_{dw}$, $\boldsymbol{F}_d$, $\boldsymbol{F}_B$ and $\boldsymbol{F}_l$ are the mass, velocity, magnetic force, downward force, drag force, Brownian force and lift force of the WBC@IMNPs, respectively. In this way, the magnitude and direction of the WBC@IMNPs' acceleration are governed by the sum of aforementioned forces. In term of magnitude of these forces (Hejazian et al., 2015), in our flyover style microfluidic chip, the drag force and magnetic force are dominant forces for WBC@IMNPs in the lateral separation zone (Fig. 1A). Similarly, the dominant forces are drag force, downward force and magnetic force (Fig. 1B) for WBC@IMNPs in the vertical separation zone.

The downward force $\boldsymbol{F}_{dw}$, which is the sum of gravity and buoyancy, can be expressed as:

$$\boldsymbol{F}_{dw} = V_c(\rho_c - \rho_f)\boldsymbol{g} \quad (2)$$

Where V_c and ρ_c are the volume and density of a WBC@IMNPs, ρ_f is the density of surrounding fluid, and $\boldsymbol{g}$ is the gravitational acceleration, respectively.

According to the Stokes' law, the drag force $\boldsymbol{F}_d$ acting on a WBC@IMNPs in the microfluidic chip is (Furlani, 2006):

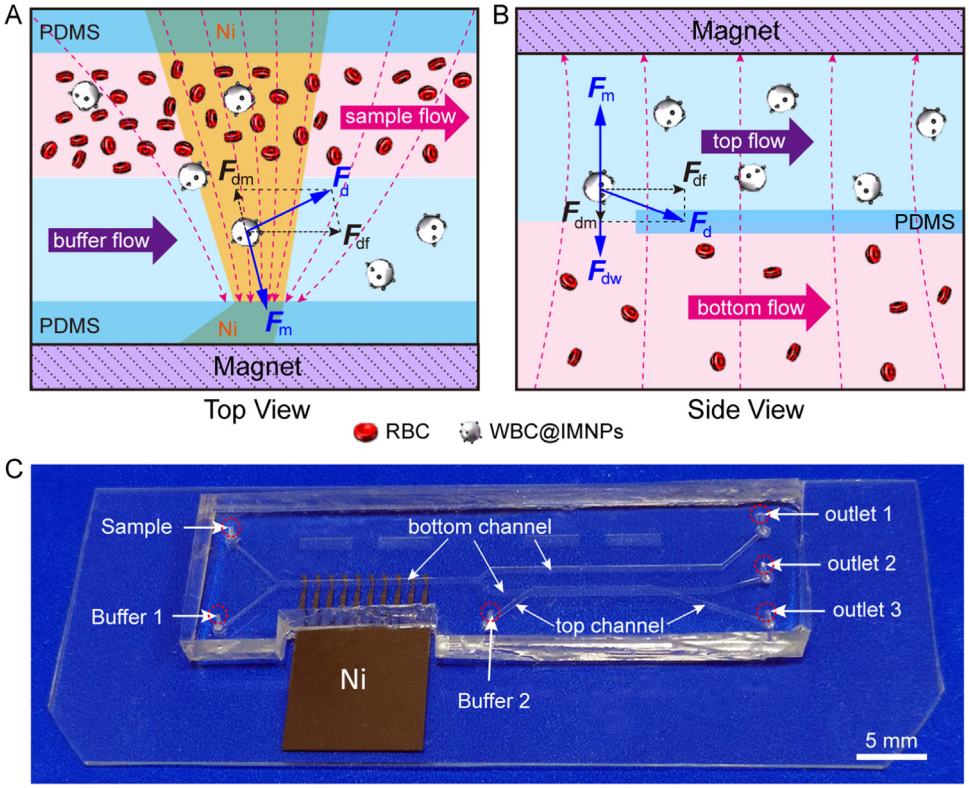

Fig. 1. Dominant forces act on a WBC@IMNPs complex in a laminar flow. (A) Representative illustration of main forces in lateral separation zone. (B) Forces acted on a complex in vertical separation zone. (C) Photograph of the flyover style microfluidic chip without placing magnets.

$$\boldsymbol{F}_d = 3\pi\eta d_c(\boldsymbol{u}_f - \boldsymbol{u}_c) \quad (3)$$

Where η and u_f are the dynamic viscosity and velocity of the fluids, d_c and u_c are the diameter and velocity of the WBC@IMNPs. When WBC@IMNPs move in the flow under a magnetic force, the drag force consists of two component forces ($\boldsymbol{F}_{dm}$ and $\boldsymbol{F}_{df}$). The $\boldsymbol{F}_{df}$ is caused by the fluid flow and bring the WBC@IMNPs toward outlets, the $\boldsymbol{F}_{dm}$ is another resistance in opposing the magnetic force direction when WBC@IMNPs move toward the magnet.

Within the microfluidic chip, the magnetic force $\boldsymbol{F}_m$ acting on a IMNP can be approximately calculated as (Gijs et al., 2010; Nguyen, 2011):

$$\boldsymbol{F}_m = \frac{V_c(\chi_p - \chi_f)}{\mu_0}(\boldsymbol{B}\cdot\nabla)\boldsymbol{B} \quad (4)$$

Where V_c is the volume of the IMNP, χ_p and χ_f are the magnetic susceptibilities of the IMNP and the fluid, the physical constant μ_0 is the permeability of vacuum, $\boldsymbol{B}$ is magnetic flux density, respectively.

2.2. Design principle

In this work, the two-stage of magnetic cells separation was consisted of lateral separation stage and vertical separation stage. The primary lateral stage was designed to enrich target cells with high recovery rate, and the vertical separation stage was used to purify enriched target cells from the lateral stage (Fig. 2A). At the lateral separation zone, a nickel micro-array (NMA) of special structure was proposed to significantly enhance local magnetic field and magnetic field gradient for separating as many target cells as possible from whole blood sample. According to Eq. (4), a greater local magnetic force in microchannel can be generated by the NMA. Thus, the higher recovery rate and separation efficiency of target cells can be guaranteed. At this stage, target cells and a fraction of unconcerned cells may move into buffer flow from sample flow(Figs. 1A, 2B). After that, when these cells enriched by the first stage within buffer flow arrived at the vertical separation zone of a flyover structure, the target cells were lifted by magnetic force and flowed into top microchannel, while the unconcerned cells continuously flowed pass the vertical separation zone in the bottom microchannel under the action of downward force and drag force (Figs. 1B, 2B). Finally, highly purified target cells were collected at outlet 3.

3. Materials and methods

3.1. Microfluidic-chip fabrication

The flyover style microfluidic chip was composed of a glass substrate and a PDMS cover. A 200 nm thick nickel (Ni) structure in a comb pattern (Fig. 2A) was deposited on a glass substrate (7.6 cm × 2.6 cm). The PDMS cover with a flyover style microchannel (heights of bottom and top channels were both 100 μm) was fabricated by soft lithography. The glass substrate was bonded with the PDMS cover after oxygen plasma surface treatment. Subsequently, the whole microfluidic chip was baked at 70 °C for 2 h to achieve an irreversible bonding (Fig. 1C). The more detailed fabrication information can be found in Supporting Information (Fig. S1, Supporting Information).

3.2. IMNPs preparation

CD45 is a specific surface marker of WBCs. Hence, magnetic micro/nano-particles (MNPs) (AllMag, Shanghai Allrun Nano Science & Technology Co., Ltd., China) were conjugated with anti-CD45 antibodies (eBioscience, USA) for specific WBCs separation. The zeta-potential of core/shell Fe_3O_4@polymer magnetic micro/nano-particles (MNPs) is about −35 mV in pH = 7.4. Typically, 1 mL of carboxylic MNPs (average diameter ~ 750 nm) suspension (2 mg mL^{-1}) were

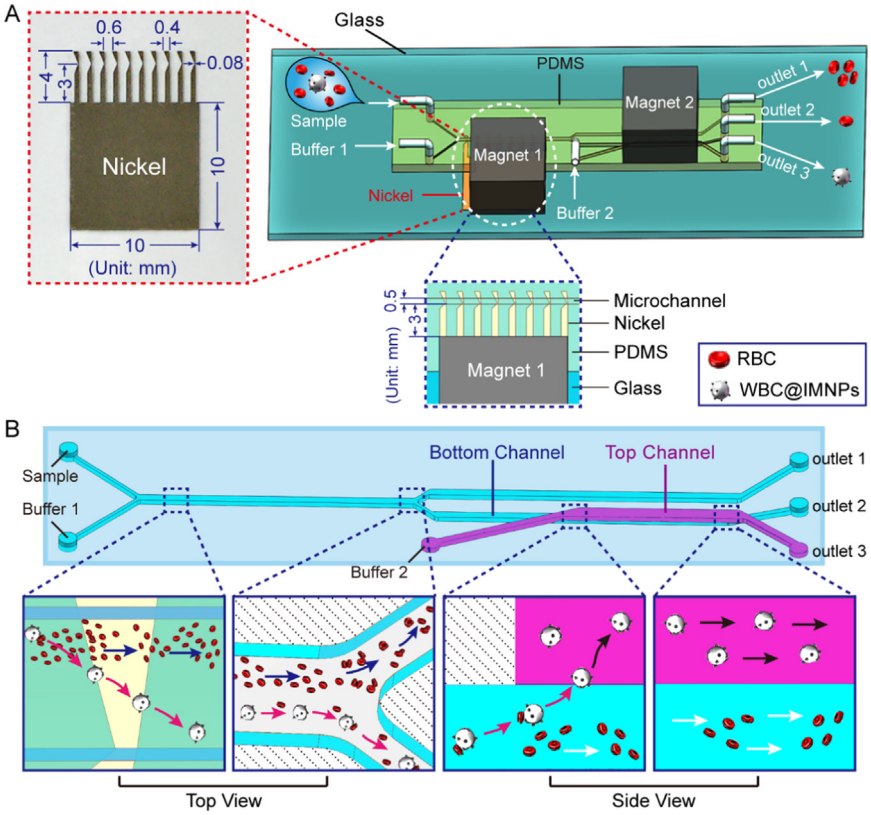

Fig. 2. Magnetic cells separation system based on a continuous-flow microfluidic chip. (A) A 3D schematic of the flyover microfluidic chip. (B) Two-stage cells separation strategy of the flyover structure microfluidic-chip.

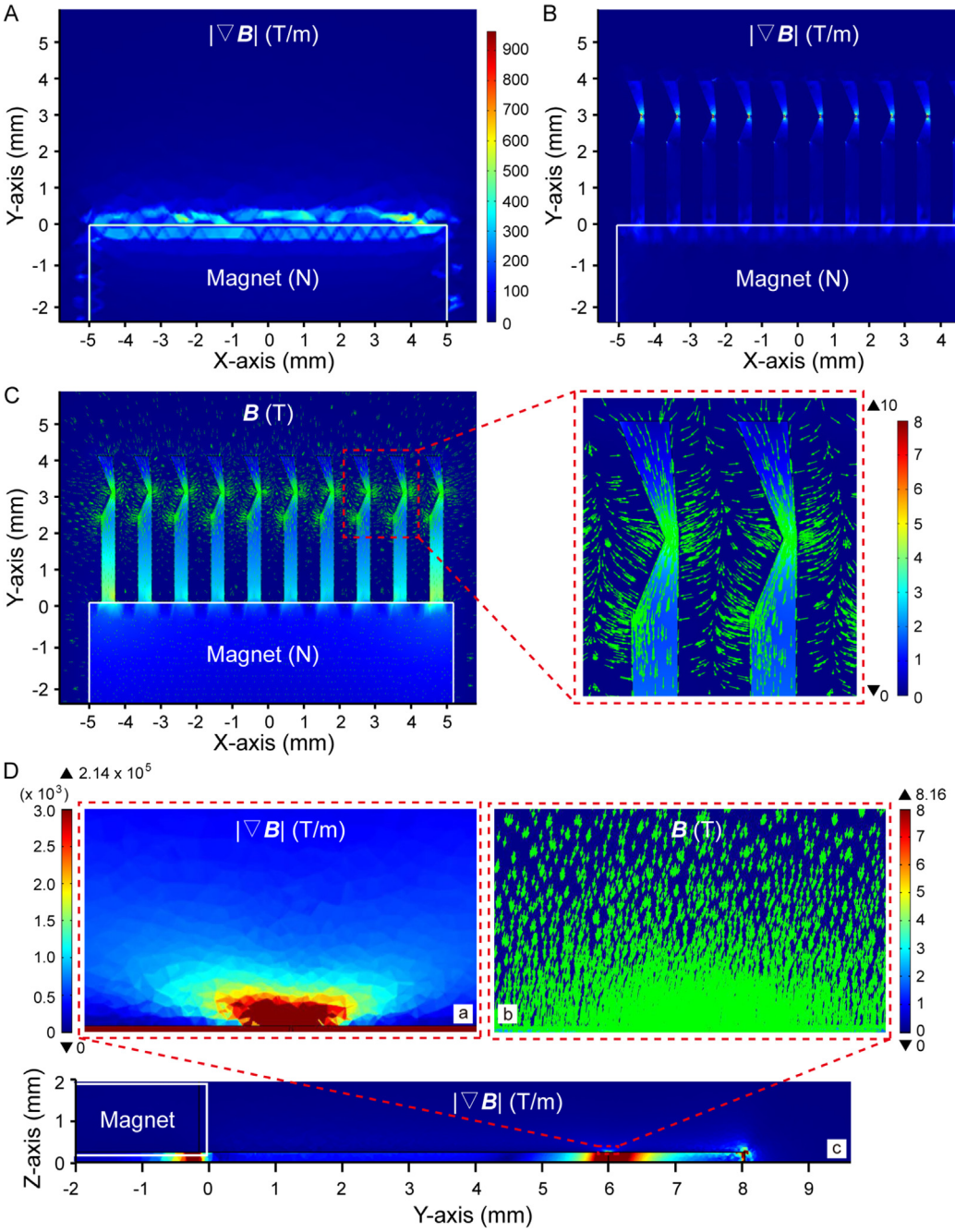

Fig. 3. Numerical simulations of the magnetic field and magnetic field gradients of the NMA (Top View). The external magnetic field of NdFeB was $\boldsymbol{B}$ = 0.3 T. (A) The distribution of magnetic field gradients of the NdFeB magnet. (B) An abrupt change in architectures of NMA created huge magnetic field gradients. The magnitude of this gradient was up to 10^5 T/m. (C) Magnetic field distribution of Ni strips. (D) The distribution of magnetic field gradients (a, c) and magnetic field (b) of the Ni strips.

activated using 1 mg of EDC and 1.3 mg of Sulf-NHS (all from Thermo, USA) for 15 min at room temperature. Then, activated MNPs were washed five times with phosphate buffer solution (PBS, pH = 7.4). Text, 40 μg of anti-mouse CD45 antibodies were gently mixed with 2 mg of activated MNPs in PBS for 2 h at 25 °C to form IMNPs (Fig. S2, Supporting Information). After that, the resultants were washed three times with PBS (pH = 7.4) to remove unreacted antibodies. Finally, the IMNPs were stored in PBS containing 0.05% (v/v) Tween 20 (pH = 7.4) at 4 °C (Zhi et al., 2014, 2012).

3.3. Experiment preparation

To realize high-purity and high-recovery rate of cells sorting, a system was assembled with a microscope, a flyover style microfluidic chip and two syringe pumps (Fig. S3, Supporting Information). The microscope was used for recording the motion trails of cells, which was consisted of a high magnification zoom lens (Zoom 6000, Navitar, USA), a microscope objective (MPLFLN 10 × 0.25 NA, Olympus, Japan) and a high-resolution camera (acA1600-28uc, Blaser, Germany). Syringe pumps were employed to precisely injected cell suspension and PBS into the flyover style microfluidic chip. Two permanent magnets (magnetic flux density: 0.3 T) were placed and stabilized at the given

positions to provide external magnetic flied for magnetic cells separation.

3.4. Separation of WBCs from mice whole blood

Mice white blood cells were used to evaluate the separation efficiency of our microfluidic-chip. Animal experiments were approved by the Ethics Committee for Animal Experiments of the Shanghai Veterinary Institute of the Chinese Academy of Agricultural Sciences, and comply with the law on animal experiments in China. The BALB/c mice (7 weeks, 20 ± 2 g) were purchased from Shanghai Experimental Animal Center, Chinese Academy of Sciences. All animal experiments were carried out in accordance with the protocol approved by the Ethics Committee of Shanghai Jiao Tong University. Whole blood samples were collected into blood collection tubes containing anticoagulant of EDTA (BD Biosciences) from the orbital sinus of mice (Qu et al., 2008). Firstly, 0.5 mL of whole blood sample was diluted in PBS (1:5, v/v). Then, 500 μL of diluted blood cell sample was mixed gently with 50 μL of prepared IMNPs suspension. After incubation for 30 min at 37 °C, the mixture was injected into microfluidic chip at different flow rate (20, 30, 40, 50, 60 μL min^{-1}). In order to make sure the cell mixture stream wouldn't displace into the recovery outlet, the flow rate ratio of the mixture to PBS was 4:5. The separation experiments were repeated three times. And, all results are reported as means ± S.D. (n = 3). All statistical analyses were done with *SPSS* 22.0 (IBM Corp., USA).

4. Results and discussion

4.1. High-precision control of magnetic force

Magnetic cell continuous sorting device generally depends on the capability of precise control of hydrodynamic force and magnetic force. In this work, control of the two forces was achieved in following two ways. First, a flyover style microchannel was designed to create a laminar flow for precise control of hydrodynamic force. This made sure that target cells can be correctly moved into recovery outlet (outlet 3) and unconcerned cells can go out through waste outlet (outlet 1 and 2). Second, for precise control of magnetic force, a Ni structure extending into microchannel was used to strengthen local magnetic field and magnetic field gradient through guiding magnetic lines of an external neodymium-iron-boron (NdFeB) permanent magnet. To optimize Ni structure, the magnetic field gradient of the Ni structure was numerically calculated using finite element analysis software (COMSOL Multiphysics 5.2, COMSOL Inc., Stockholm, Sweden). In numerical calculations, several key parameters were relative magnetic permeability ($\mu_{r,\ nickel} = 200$, $\mu_{r,\ air} = 1.05$) (Adams et al., 2008) and magnetic field strength ($\boldsymbol{B} = 0.3$ T) of the NdFeB magnet. In contrast to magnetic field gradient (< 1000 T/m) of only magnet (Fig. 3A), the highest magnetic field gradient was 2×10^5 T/m at the corner of the Ni strip on XY plane (Fig. 3B), which confirming that the designed Ni architecture can tremendously amplify local magnetic field gradient in microchannel. Furthermore, as shown in Fig. 3C (XY plane), magnetic field lines in the microchannel were focused on the corners of the Ni strips. Meanwhile, as shown in Fig. 3D (YZ plane), in comparison with straight Ni strips, magnetic field gradient and magnetic field on YZ plane also were enhanced at the corners of Ni strips. The results also indicated that the magnetic force on an IMNP was up to several nanonewtons (calculated via Eq. (4)). This magnetic force was sufficient to sort target cells at lateral direction and made sure nearly all of the labeled cells were sorted (Adams et al., 2008).

4.2. Characterization of IMNPs

The characterization of IMNPs was performed by UV–vis spectra (Cary-50 UV–vis spectrometer, Agilent, USA), Fourier transform infrared spectra (FTIR) (EQUINOX 55, Bruker, Germany) and magnetic property (PPMS-9T (EC-II), Quantum Design, USA). The UV − vis spectra of MNPs (Fig. S4B, Supporting Information, blue line) shows the strong absorption peak at 540 nm. After modification with CD45 antibodies (Fig. S4B, Supporting Information, red line), the strong absorption peak shifted from 540 to 580 nm, the 40 nm blue shift owing to the change of the MPNs electronic ground state induced by antibodies conjugation. Compared with MNPs, the spectrum of the IMNP (Fig. S4C, Supporting Information) shows that the CHN deformation vibration peak at 1544 cm^{-1} (amide II vibration) appeared, which was due to the amide bond in the infrared spectrum (Meng et al., 2016). It confirmed that anti-mouse CD45 antibodies have been bonded to the surface of the

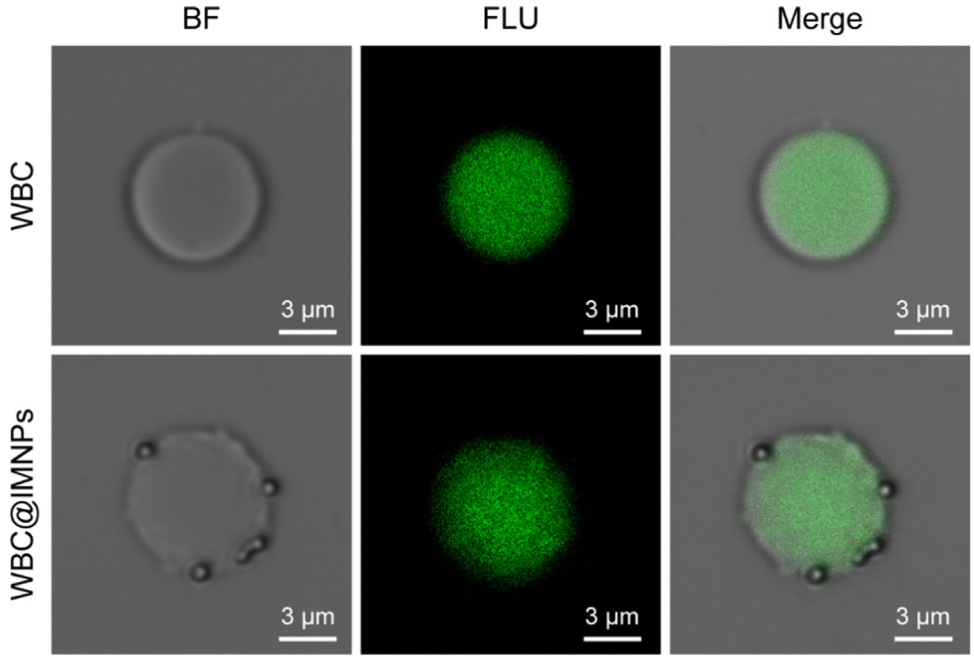

Fig. 4. LSCM image of CD45-FITC labeled WBCs and IMNPs CD45-FITC labeled WBCs at bright field (BF) and fluorescence (FLU) situations. From the BF and merge images, the IMNPs were clearly labeled on the surface of the WBCs.

carboxylic MNPs. And the C=C stretching vibration peak at 1437 cm^{-1} of polystyrene coating of MNPs significantly decreased, which was ascribed to antibodies bonded on the surface of MNPs. The formation of IMNPs was confirmed by UV–Vis (Fig. S4B, Supporting Information) and FTIR spectra (Fig. S4C, Supporting Information). According to the plots of magnetization versus magnetic field (M-H loop) of the MNPs and IMNPs, it is apparent that there is obvious no hysteresis, both remanence and coercivity are almost zero, suggesting that MNPs and IMNPs are superparamagnetic (Fig. S4D, Supporting Information). The maximum saturation magnetization (*Ms*) of MNPs and IMNPs were 42.8 emu·g^{-1} and 26.5 emu·g^{-1} at 300 K, respectively.

4.3. Specific labeling of IMNPs on WBCs

In this study, the critical factor to influence high-purity magnetic separation is specificity of IMNPs. Accordingly, we firstly assessed performance of IMNPs for specific-targeting WBCs by scanning electron microscope (SEM) and laser scanning confocal microscopy (LSCM). It was found that several IMNPs specifically bond on the surface of WBCs (Fig. S5B, Supporting Information) and none of IMNPs bond on RBCs (Fig. S5C, Supporting Information). Moreover, different sizes of IMNPs have different effects on WBCs. Small diameter IMNPs (180 nm) were easily swallowed up by WBCs (Fig. S5D, Supporting Information). According to the magnetization principle, the larger diameter of the IMNPs can obtain larger magnetic forces than the smaller ones at the same magnetic field. Nevertheless, too large IMNPs (1100 nm diameter) deposited rapidly in syringe and polyfluortetraethylene tubes, resulting in a decrease in cell recovery rate. Thus, appropriate diameter (750 nm) of IMNPs were suitable for magnetic cell sorting in this work (Bohmer et al., 2017).

4.4. Separation of WBCs from peripheral blood

After two-stage magnetic separation of lateral separation (Movie S1, Supporting Information) and vertical separation (Movie S2 and Fig. S6, Supporting Information), the separated WBCs were fluorescently labeled with anti-mouse CD45-FITC antibodies (Affymetrix eBioscience Inc., USA). As shown in Fig. 4, the LSCM results further confirmed that the IMNPs specifically labeled on the surface of the WBCs recovered from outlet 3.

Supplementary material related to this article can be found online at doi:10.1016/j.bios.2018.12.058.

To assess the sorting performance of this flyover style microfluidic chip, WBCs in whole blood were separated at different flow rates (20, 30, 40, 50, 60 μL min^{-1}) in it. Then, the magnetic separated WBCs were fluorescently labeled with anti-mouse CD45-FITC antibodies. The positive rates of WBCs were analyzed by FACS Calibur (Becton Dickinson, USA). As shown in Fig. 5A and B, the purities of separated WBCs gradually descended with increased flow rate. For the single stage magnetic separation (Fig. 5A), the separation purities of WBCs were 84.3 ± 1.76%, 81.7 ± 2.13%, 78.2 ± 2.58%, 74.5 ± 3.03% and 70.2 ± 3.69% at the flow rates of 20, 30, 40, 50 and 60 μL min^{-1}, respectively. And, the separation purities from two-stage magnetic separation were 93.2 ± 1.67%, 90.3 ± 2.02%, 87.1 ± 2.35%, 82.8 ± 2.86% and 78.2 ± 3.37% at the flow rates of 20, 30, 40, 50 and 60 μL min^{-1}, respectively (Fig. 5B). The positive rates of WBCs were more than 90% at flow rate of 20 and 30 μL min^{-1}. A comparison of the two groups results showed obvious statistical differences at flow rates of 20, 30, 40 and 50 μL min^{-1}, but the statistical difference disappeared at the flow rate of 60 μL min^{-1}. This proved that two-stage magnetic separation significantly excelled the single stage magnetic separation due to introduction of vertical magnetic force. Nevertheless,

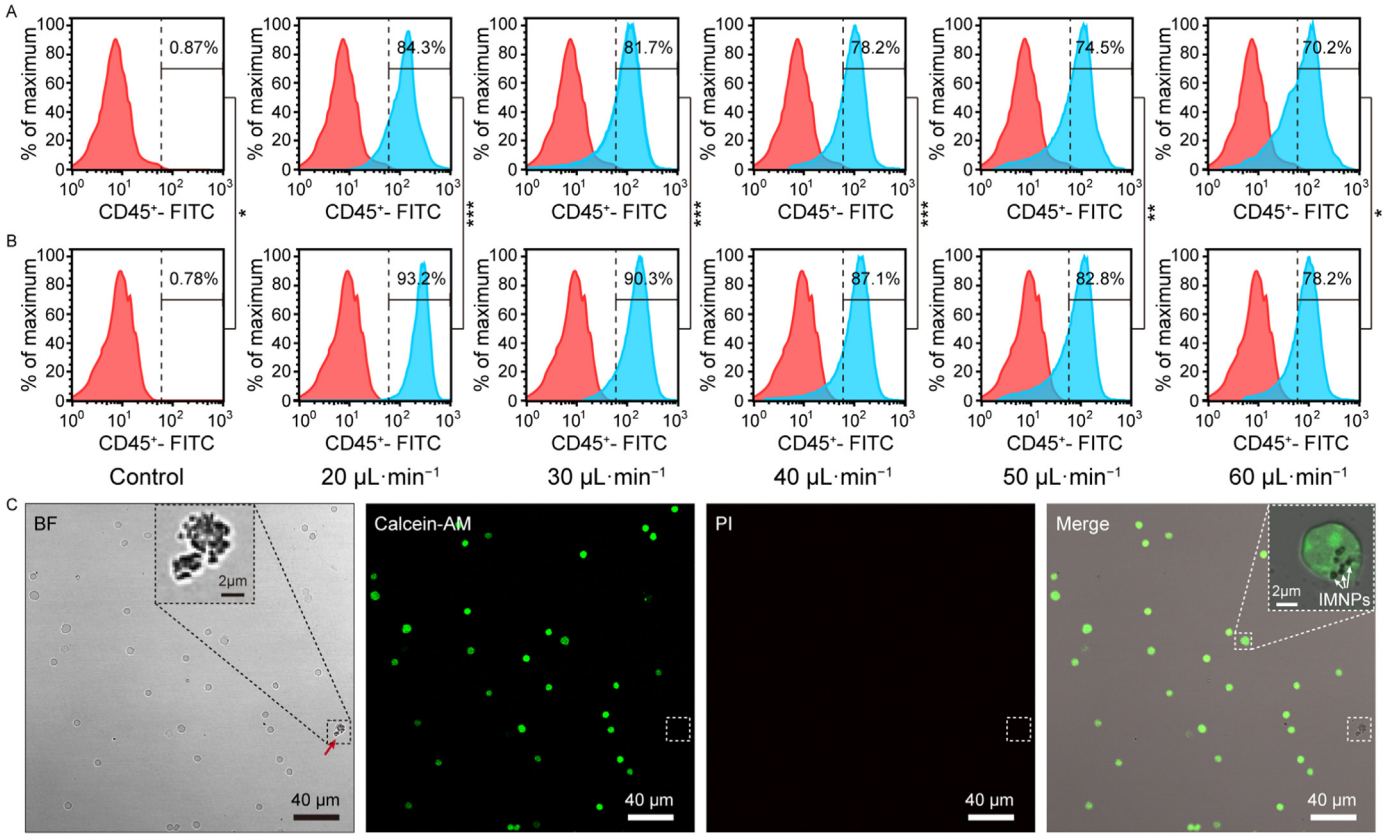

Fig. 5. Validation of magnetic sorting performance of the flyover style microfluidic chip. (A) The separation purities of WBCs through single one-stage magnetic separation at different flow rates (lateral separation). (B) The separation purities of WBCs through two-stage magnetic separation at different flow rates. (C) Viability assess of two-stage magnetic separated WBCs. (* $P > 0.05$, ** $P < 0.05$, *** $P < 0.01$).

Reynolds numbers will become bigger with flow rate increase. The high Reynolds numbers consequently led to low separation purity (Adams et al., 2008). In addition, flat RBCs flow fast in the microchannel, the moment and the physical center did not coincide, which maybe cause the lateral and vertical movements of the RBCs to decrease separation purity. Finally, the viability of separated WBCs was assessed by means of a dual staining technique using a calcein acetoxymethyl ester (calcein-AM) and other propidium iodide (PI) (Thermo Fisher Scientific, USA). The staining was carried out according to the protocol. Statistically, the rate of survival separated WBCs was 97.5 ± 1.8%. As shown in Fig. 5C, only one WBC was dead and cracked (red arrow), and IMNPs were observed on the surfaces of WBCs. The high rate of survival also indicated that the high magnetic field did not damaged the WBCs.

Increasing the magnetic field gradient is helpful to achieve both high efficiency and throughput of magnetically labeled cells. Jung and Han (2008) ever laid ferromagnetic wire array in a straight microchannel of microfluidic chip to improve the separation efficiency and throughput of WBCs from peripheral whole blood. Ultimately, the WBCs separation efficiency and purity were 89.2% and 1.45% at flow rate of 20 μL h^{-1} (~ 10^5 cell·min^{-1}) under a 0.3 T external magnetic field, respectively. Mizuno et al. (2013) introduced a microfluidic system that utilizes both hydrodynamic and magnetic forces to sort the tagged JM cells and HeLa cells based on their sizes and magnetic properties. Finally, the purification ratio was higher than 90% at the flow rate of 5 μL min^{-1} (~ 10^3 cells·min^{-1}). In comparison, our flyover style microfluidic chip has obvious superiorities with high separation purity of 93.2% and high cell viability of 97.5% at flow rate of 20 μL min^{-1} (~ 10^6 cell·min^{-1}).

5. Conclusions

In conclusion, we fabricated a flyover style microfluidic chip to achieve high-purity WBCs separation by two-stage magnetic separation in a continuous flow. Firstly, to improve the recovery of WBCs, a special-designed Ni structure was fabricated at the lateral sorting region, by which the local magnetic flied gradient can be remarkably enhanced to 10^5 T/m under a 0.3 T external magnetic flied. This guarantees that WBC@IMNPs effectively transported across the interface of the sample mixture and buffer stream. Furthermore, a flyover-style microchannel was designed to obtain higher purity of WBCs at the second-stage vertical magnetic separation. The experimental results showed that purity of separated WBCs reached to 93.2 ± 1.67% at flow rate of 20 μL min^{-1} and the viability rate of separated WBCs was 97.5 ± 1.8%. In summary, we successfully developed a flyover style microfluidic chip for separating and purifying WBCs from whole blood by two-stage magnetic separation in a continuous flow. This microfluidic chip has a great potential application of WBCs or subtype of WBCs separation and even negative enrichment of rare circulating tumor cells in the field of clinical diagnosis.

Acknowledgments

This work was financially supported by the Science and Technology Commission of Shanghai Municipality (No. 15441904800), Economy and Informatization Technology Commission of Shanghai Municipality (No. XC-ZXSJ-02-2016-05), National Key Research and Development Program of China (Nos. 2016YFC0100902 and 2017YFA0205301), Open Fund of State Key Laboratory of Pathogenic Microorganism Biosafety (No. SKLPBS1827) and Chinese Ministry of Science and Technology (No. 2017ZX10203205-006-002). It was carried out in Center for Advanced Electronic Materials and Devices (AEMD) of Shanghai Jiao Tong University.

Appendix A. Supplementary material

Supplementary data associated with this article can be found in the online version at doi:10.1016/j.bios.2018.12.058.

References

Abdulla, A., Liu, W., Gholamipour-Shirazi, A., Sun, J., Ding, X., 2018. Anal. Chem. 90, 4397–4405.
Adams, D.L., Zhu, P., Makarova, O.V., Martin, S.S., Charpentier, M., Chumsri, S., Li, S., Amstutz, P., Tang, C.M., 2014. RSC Adv. 9, 4334–4342.
Adams, J.D., Kim, U., Soh, H.T., 2008. PNAS 105, 18165–18170.
Ahmed, M.G., Abate, M.F., Song, Y., Zhu, Z., Yan, F., Xu, Y., Wang, X., Li, Q., Yang, C., 2017. Angew. Chem. Int. Ed. 56, 10681–10685.
Bhuvanendran Nair Gourikutty, S., Chang, C.P., Puiu, P.D., 2016. J. Chromatogr. B Anal. Technol. Biomed. Life Sci. 1011, 77–88.
Bohmer, N., Demarmels, N., Tsolaki, E., Gerken, L., Keevend, K., Bertazzo, S., Lattuada, M., Herrmann, I.K., 2017. ACS Appl. Mater. Interfaces 9, 29571–29579.
Brunstein, C.G., Miller, J.S., McKenna, D.H., Hippen, K.L., DeFor, T.E., Sumstad, D., Curtsinger, J., Verneris, M.R., MacMillan, M.L., Levine, B.L., 2015. Blood 127, 1044–1051.
Chen, J., Chen, D., Yuan, T., Chen, X., Xie, Y., Fu, H., Cui, D., Fan, X., Khaing, Oo, M.K., 2014. Microelectron. Eng. 128, 36–41.
Chen, X., Liang, Z., Li, D., Xiong, Y., Xiong, P., Guan, Y., Hou, S., Hu, Y., Chen, S., Liu, G., Tian, Y., 2018. Biosens. Bioelectron. 99, 416–423.
Delong, T., Wiles, T.A., Baker, R.L., Bradley, B., Barbour, G., Reisdorph, R., Armstrong, M., Powell, R.L., Reisdorph, N., Kumar, N., Elso, C.M., DeNicola, M., Bottino, R., Powers, A.C., Harlan, D.M., Kent, S.C., Mannering, S.I., Haskins, K., 2016. Science 351, 711–714.
Ding, X., Lin, S.C., Kiraly, B., Yue, H., Li, S., Chiang, I.K., Shi, J., Benkovic, S.J., Huang, T.J., 2012. PNAS 109, 11105–11109.
Doitsh, G., Galloway, N.L.K., Geng, X., Yang, Z., Monroe, K.M., Zepeda, O., Hunt, P.W., Hatano, H., Sowinski, S., Muñoz-Arias, I., Greene, W.C., 2013. Nature 505, 509–516.
Furlani, E.P., 2006. J. Appl. Phys. 99, 024912.
Gholizadeh, S., Shehata Draz, M., Zarghooni, M., Sanati-Nezhad, A., Ghavami, S., Shafiee, H., Akbari, M., 2017. Biosens. Bioelectron. 91, 588–605.
Gijs, M.A.M., Lacharme, Fdr, Lehmann, U., 2010. Chem. Rev. 110, 1518–1563.
Gossett, D.R., Weaver, W.M., Mach, A.J., Hur, S.C., Tse, H.T.K., Lee, W., Amini, H., Di Carlo, D., 2010. Anal. Bioanal. Chem. 397, 3249–3267.
Haber, C., Wirtz, D., 2000. Rev. Sci. Instrum. 71, 4561–4570.
Hejazian, M., Li, W., Nguyen, N.T., 2015. Lab Chip 15, 959–970.
Hyun, K.A., Lee, T.Y., Lee, S.H., Jung, H.I., 2015. Biosens. Bioelectron. 67, 86–92.
Iranmanesh, M., Hulliger, J., 2017. Chem. Soc. Rev. 46, 5925–5934.
Jeorrett, A.H., Neale, S.L., Massoubre, D., Gu, E., Henderson, R.K., Millington, O., Mathieson, K., Dawson, M.D., 2014. Opt. Express 22, 1372–1380.
Joyce, J.A., Fearon, D.T., 2015. Science 348, 74–80.
Jung, J., Han, K.-H., 2008. Appl. Phys. Lett. 93, 223902.
Kim, B., Choi, Y.J., Seo, H., Shin, E.C., Choi, S., 2016. Small 12, 5159–5168.
Lipfert, J., Hao, X., Dekker, N.H., 2009. Biophys. J. 96, 5040–5049.
Liu, C., Stakenborg, T., Peeters, S., Lagae, L., 2009. J. Appl. Phys. 105, 102014.
Maini, M.K., Boni, C., Lee, C.K., Larrubia, J.R., Reignat, S., Ogg, G.S., King, A.S., Herberg, J., Gilson, R., Alisa, A., 2000. J. Exp. Med. 191, 1269–1280.
Meng, C., Zhi, X., Li, C., Li, C., Chen, Z., Qiu, X., Ding, C., Ma, L., Lu, H., Chen, D., 2016. ACS Nano 10, 2203–2213.
Mizuno, M., Yamada, M., Mitamura, R., Ike, K., Toyama, K., Seki, M., 2013. Anal. Chem. 85, 7666–7673.
Nguyen, N.T., 2011. Microfluid. Nanofluid. 12, 1–16.
Nivedita, N., Papautsky, I., 2013. Biomicrofluidics 7, 054101.
Osman, O., Toru, S., Dumas-Bouchiat, F., Dempsey, N.M., Haddour, N., Zanini, L.F., Buret, F., Reyne, G., Frenea-Robin, M., 2013. Biomicrofluidics 7, 54115.
Plouffe, B.D., Murthy, S.K., 2014. Anal. Chem. 86, 11481–11488.
Plouffe, B.D., Murthy, S.K., Lewis, L.H., 2014. Rep. Prog. Phys. 78, 016601.
Poudineh, M., Labib, M., Ahmed, S., Nguyen, L.N.M., Kermanshah, L., Mohamadi, R.M., Sargent, E.H., Kelley, S.O., 2017. Angew. Chem. Int. Ed. 56, 163–168.
Qu, B.Y., Wu, Z.Y., Fang, F., Bai, Z.M., Yang, D.Z., Xu, S.K., 2008. Anal. Bioanal. Chem. 392, 1317–1324.
Russom, A., Gupta, A.K., Nagrath, S., Di Carlo, D., Edd, J.F., Toner, M., 2009. New J. Phys. 11, 75025.
Serrano-Villar, S., Sainz, T., Lee, S.A., Hunt, P.W., Sinclair, E., Shacklett, B.L., Ferre, A.L., Hayes, T.L., Somsouk, M., Hsue, P.Y., Van Natta, M.L., Meinert, C.L., Lederman, M.M., Hatano, H., Jain, V., Huang, Y., Hecht, F.M., Martin, J.N., McCune, J.M., Moreno, S., Deeks, S.G., 2014. PLoS Pathog. 10, e1004078.
Wang, X., Chen, S., Kong, M., Wang, Z., Costa, K.D., Li, R.A., Sun, D., 2011. Lab Chip 11, 3656–3662.
Warkiani, M.E., Wu, L., Tay, A.K., Han, J., 2015. Annu. Rev. Biomed. Eng. 17, 1–34.
Welzel, G., Seitz, D., Schuster, S., 2015. Sci. Rep. 5, 7959.
Wu, L., Guan, G., Hou, H.W., Bhagat, A.A., Han, J., 2012. Anal. Chem. 84, 9324–9331.
Wu, Z., Chen, Y., Wang, M., Chung, A.J., 2016. Lab Chip 16, 532–542.
Yu, Z.T.F., Aw Yong, K.M., Fu, J., 2014. Small 10, 1687–1703.
Zeng, J., Deng, Y., Vedantam, P., Tzeng, T.-R., Xuan, X., 2013. J. Magn. Magn. Mater. 346, 118–123.
Zhang, Q., Yin, T., Xu, R., Gao, W., Zhao, H., Shapter, J.G., Wang, K., Shen, Y., Huang, P., Gao, G., Wu, Y., Cui, D., 2017. Nanoscale 9, 13592–13599.
Zhi, X., Deng, M., Yang, H., Gao, G., Wang, K., Fu, H., Zhang, Y., Chen, D., Cui, D., 2014. Biosens. Bioelectron. 54, 372–377.
Zhi, X., Liu, Q., Zhang, X., Zhang, Y., Feng, J., Cui, D., 2012. Lab Chip 12, 741–745.